International Journal of Physical Sciences

Volume 11 Number 24 30 December , 2016

ISSN 1992-1950

Academic Journals

ABOUT IJPS

The **International Journal of Physical Sciences (IJPS)** is published weekly (one volume per year) by Academic Journals.

International Journal of Physical Sciences (IJPS) is an open access journal that publishes high-quality solicited and unsolicited articles, in English, in all Physics and chemistry including artificial intelligence, neural processing, nuclear and particle physics, geophysics, physics in medicine and biology, plasma physics, semiconductor science and technology, wireless and optical communications, materials science, energy and fuels, environmental science and technology, combinatorial chemistry, natural products, molecular therapeutics, geochemistry, cement and concrete research, metallurgy, crystallography and computer-aided materials design. All articles published in IJPS are peer-reviewed.

Contact Us

Editorial Office: ijps@academicjournals.org

Help Desk: helpdesk@academicjournals.org

Website: http://www.academicjournals.org/journal/IJPS

Submit manuscript online http://ms.academicjournals.me/

Editorial Board

International Journal of Physical Sciences

Table of Contents: Volume 11 Number 24, 30 December, 2016

ARTICLES

academicJournals

Vol. 11(24), pp. 326-335, 30 December, 2016
DOI: 10.5897/IJPS2016.4551
Article Number: 916DF7C62066
ISSN 1992 - 1950

http://www.academicjournals.org/IJPS

International Journal of Physical Sciences

Full Length Research Paper

Numerical modeling and determination of parameters characteristic of a photovoltaic module LRAER (FST Nouakchott)

M. M. Menou[1,3]*, A. Yahfdhou[1,2], A. K. Mahmoud[1], A. M. Yahya[1,2] and I. Youm[2,3]

[1]Applied Research Laboratory for Renewable Energies, LRAER, University of Science and Technology and Medicine, in Nouakchott, Mauritania.
[2]Laboratory of Semiconductor and Solar Energy, LASES, Faculty of Science and Technology, University Cheikh Anta Diop, Dakar, Senegal.
[3]Studies and Research Center of Renewable Energies ' CERER ', Dakar, Senegal.

Received 15 August, 2016; Accepted 11 November, 2016

The main objective of this work is to study, develop and establish an approach through the mathematical model of performance CENERG under the term (MC). This model is used to characterize the parameters of photovoltaic systems in the literature. For this, we have considered the required performance is normally measured in standard test conditions (STC), where an average solar spectrum AM 1.5 is used, sunshine is normalized at 1000 W/m², and the cell temperature is set equal to 25°C. Modeling which is presented based on data provided by the manufacturers of solar cells or panels. The mathematical modeling process is performed with the model (MC) in search of the equations governing the operation of LRAER group photovoltaic panels, to that end, we can determine the parameters of the mathematical model (MC). The work also allows showing accuracies, through the comparison of the simulation results obtained with the actual production data (experimental) to ATERSA 75 W modules of the LRAER USTM.

Key words: PV generator model (GPV), CENERG mathematical model, characteristics I (V), characteristics P(V).

INTRODUCTION

The mathematical model proposed for the realization of this work is that of CENERG. This model was validated experimentally by the Energy Center in Sophia Antipolis (Chenni et al., 2007). The most important thing to remember for this model is that it provides a method to calculate the PV module performance from data provided by the manufacturers (Belhadj et al., 2010).

Thus, with this model, we propose a study to highlight the influence of several parameters (temperature, Rs resistance, resistance Rsh and sunshine) for the

*Corresponding author. E-mail: hakim.menou@live.fr. Tel: +22236303457.

determination of the characteristic I(V) and P(V) through the simulation of all the characteristics of the GPV. Each time, it will be proposed in this work a comparison between simulation results and those of the manufacturer for the test module ATERSA 75 W, looking for accuracy, compliance results with those known in the literature (Khazzar and Zereg, 2010; Bonkoungou et al., 2013; Zhou et al., 2007; El Ouariachi et al., 2009). For this, it will be conducted comparing the results obtained by simulation (MC) and the experimental results. In addition, it will be added to this job just at the end, a comparison in terms of errors between the simulation of the power of the numerical model and the results of experimentally recorded parameters on LRAER site.

Thereafter, it will be checked behavior through the comparison of errors between the experimental and simulated powers during the most remarkable days with those given by the experimental site, to be able to comment on the accuracy of the model Digital (MC) used in this work. In addition, this error will be expanded compared to the parameters of the photovoltaic panel manufacturer.

In the end, the discussion will be addressed on the results achieved as part of this work will be based on a comparison of the simulation results, those data by the manufacturer and those recorded by the experimental site.

METHODOLOGY

Experimental device LRAER

The experimental device is designed to give it the electrical energy from two sources to charge the storage system to meet the demand coverage expenses.

Constituents of the experimental device

This is achieved thanks to the photovoltaic generator LRAER which consists of 16 modules (Atersa). Its configuration provides four panels (Figure 1), which are connected in series for (48 V) and then they are placed in parallel with the other groups (Yahya et al., 2011). Total peak power of the system is 1.2 kWp. The surface of the generator system is 8.6 m².

It is important to note that the capacity of the storage system (1200 Ah). The energy storage device implanted in this hybrid system is connected directly (Yahfdhou et al., 2013) to the DC bus. It therefore has 24 storage cells, of 2 V. The elements are connected in series. The DC bus is connected to AC mains via a reversible power converter 5 Kw, brand Trace Engineering SW. It will add the converter should be able to deliver higher power peaks of the load. This configuration is proposed in Figure 1.

In addition, this production system is fully automated. Various measuring sensors have been installed and allow us to obtain the data of the entire hybrid system: The speed and direction of wind, sunshine on the horizontal plane, the ambient temperature, module temperature, the electricity production of wind turbines, the electrical output of photovoltaic array, the generator and the operating voltage of the DC bus.

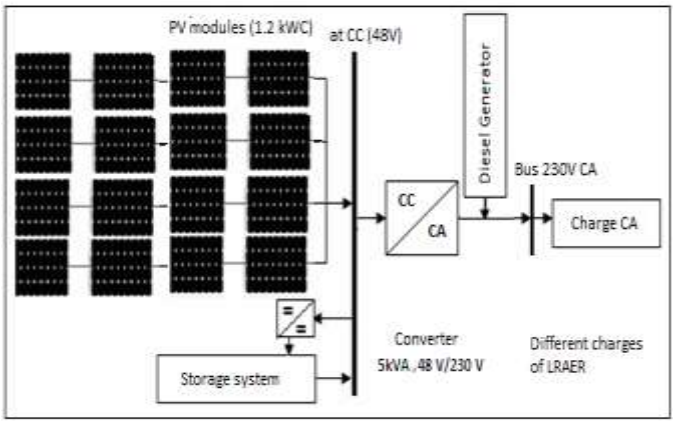

Figure 1. Hybrid system PV / diesel.

Also note that the experimental device is coupled with a desalination unit brackish water (reverse osmosis) and other equipment (computers, lighting and motors).

PV array features

Above, it is proposed to the manufacturer of the photovoltaic panel in Table 1.

Electric models of the PV generator (GPV)

In the literature, there are several electric models that describe the operation and behavior of the PV array. These models differ in the procedure calculates the precision and the number of parameters involved in the digital model.

Indeed, on the basis of the analysis of the configurations proposed in the literature (Dumbs, 1999). Two models (Model GPV diode 1 and its panel array pattern) were proposed shown in Figures 2 and 3.

In this context, the model 1 diode GPV (Figure 2) shows the physical phenomena governing most interactions related to various materials used in the panels or to a larger scale in the equivalent generator LRAER (Figure 3).

The model of Figure 2 is processed to obtain the equivalent diagram of Figure 3, as follows:

Numerical modeling models

The choice of mathematical model that simulates the behavior of photovoltaic panel is determined by the type of problems to be studied. This model can be considered simply an analysis of the influence of meteorological parameters. Similarly, the model also solves the choice of the size of the system to install. Thus, regarding the modeling of GPV, bibliographic study found the model that is developed by the Energy Center (Cenreg). This model is based in this case on the model to 1 diode.

Mathematical models MC with 1 diode

The mathematical model includes the following variables in Figure 3:

Table 1. Characteristic of the PV generator.

Specification ATERSA 1000 W/m^2 25°C AM 1.5	
Number of series	98090135
Number of panels	16
Model	AP-7105/A-75
Maximum power	75 W
Short circuit current Icc	4.8 A
Open circuit voltage Vco	21 V
Maximum current Imp	4.4 V
Maximum voltage Vmp	17 V
Dimensions	1,206 × 0,53 × 0,034m
Weight	8.2kg
Mode de connexion	4 panels (//) of 4 in series
Area used by the modules	8.6 m^2

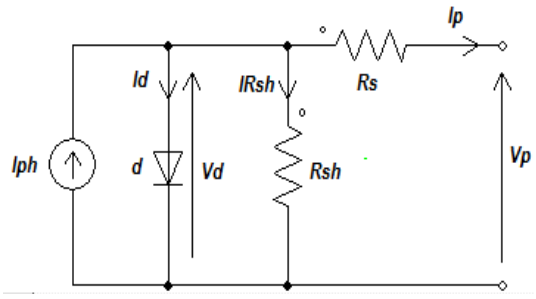

Figure 2. Model 1 diode of GPV.

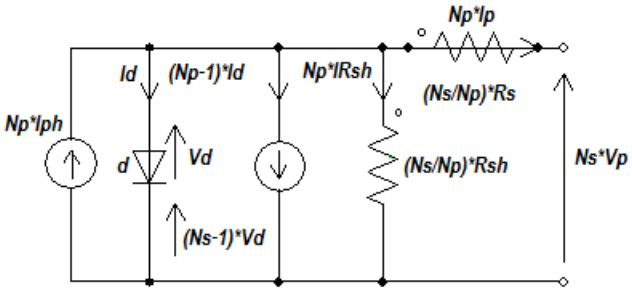

Figure 3. Model of a panel group (Single diode).

E_S: Irradiance on the panels (W / m^2),
T_j: Temperature of junction of the cells (°C)
I_G: Current of panels group (A)
V_G: Tension in the terminal group (V).

The equation that characterizes the Figure 2 of GPV will be as follows:

$$I_G = I_{Ph} - I_d - i_{rsh} \quad (1)$$

The current Iph of panels is given by the following equation:

$$I_{Ph} = P_1 E_S \left[1 + P_2\left(E_S - E_{ref}\right) + P_3\left(T_j - T_{jref}\right)\right] \quad (2)$$

Where Eref is the reference sunshine at 1000 W/m^2 and Tref is the reference temperature 25°C; P1, P2, and P3 are constant parameters.

The current passing through the diode is given by:

$$I_d = I_{Sat}\left[\exp\left(\frac{q}{kAn_S T_j}\left(V_G + R_S I_G\right)\right) - 1\right] \quad (3)$$

Where: I_{sat} = saturation current (A); q = Elementary charge (1.6*10-19 C); k = Constant of Boltzman (1.38*10-23 J/K); n_S = Number of cells; A = Ideality factor.

The saturation current:

$$I_{Sat} = P_4 T_j^3 \exp\left(-\frac{E_g}{kT_j}\right) \quad (4)$$

E_G is the energy gap and P4 is a constant parameter.

The shunt current is given as follows:

$$I_{Rsh} = \frac{V_G}{R_{sh}} \quad (5)$$

So we can write the final equation for the group as follows:

$$I_G = P_1 E_S\left[1 + P_2\left(E_S - E_{ref}\right) + P_3\left(T_j - T_{jref}\right)\right] - \frac{V_G}{R_{sh}} - P_4 T_j^3 \exp\left(-\frac{E_g}{kT_j}\right)\left[\exp\left(\frac{q}{kAn_S T_j}\left(V_G + R_S I_G\right)\right) - 1\right] \quad (6)$$

We found that this equation translates the action of the GPV and is a function of the form:

$$I_G = f\left(I_G, V_G, E_S, T_S\right) \quad (7)$$

Mathematical models MC with 1 diode for panel group

The equation of the characteristic relating to a module array is formed by the series arrangement of modules Ms and Mp parallel modules, is extrapolated from that of a photovoltaic module and is given in (Gergaud et al., 2002). Indeed, Figure 3 is used to write the equations for the panels group as follows:

$I_{ph} = N_p * I_{ph}$
$I_G = N_p * I_p$
$I_d = N_p * I_d$
$I_{Rsh} = N_p * I_{Rsh}$
$V_d = N_s * V_d$
$V_G = N_s * V_p$
$R_s = (N_s/N_p) * R_s$
$R_{sh} = (N_s/N_p) * R_{sh}$

Under these conditions, we are called to determine the Equation 6 the following seven parameters: P1, P2, P3, P4, A, Rs, Rsh. In addition, we are also called to account for the photovoltaic system requirements LRAER generation, which says the equivalent mathematical model of the LRAER system is only valid if the modules are identical and face the weather changes the same site.

MC model parameters with 1 diode

To determine the MC model parameters to 1 diode, use the input provided by the manufacturer's documentation in Table 1 and the data provided by the LRAER data acquisition system in terms of sunshine and temperatures. These data will allow achieving the extraction of parameters in the result of this work through the resolution of the Equation 6.

Extractions parameters for ATERSA 75 W

These parameters are not measurable quantities and are not usually included in the manufacturer's data. Therefore, they must be determined from the characteristics of GPV, based on actual data from the data acquisition system.

For extracting ATERSA 75 W parameters, there was used the MC model 1 diode. So that the coefficients P1, P2, P3, P4, A, R, and Rsh in equations are identified and experimentally validated. Against by the electric power of GPV be determined by calculation by multiplying the voltage V and the calculated intensity I in Equation 6. This method of extraction parameters using the experimental data of the data acquisition system enables more reliable fi characterization of the actual behavior of the GPV. Thus, the parameters of the polynomial model were determined, they were from three outstanding points are:

1. In the short-circuit current (Icc), we have (0, Icc),
2. For the open circuit voltage (Voc), we (Voc, 0),
3. For maximum power point (Vmp, Imp).

The result of the parameter identification is presented in Table 2.

Table 2. MC model parameters GPV for 1 diode.

Parameter	Value
P1	0.0048
P2	0.0001
P3	-0.0005
P4	202.5
A	1
Rs	0.28
Rsh	115.9

RESULTS OF SIMULATION

Indeed, mathematical models developed in this work will be presented Matlab to realize the different simulations in line with the objectives that were defined in the introduction. Indeed, the simulation results, their details and their agreements with the physical phenomena known to the GPV is either a validation of the numerical model (MC).

Simulation I (V) and P (V) for the model with one diode of the GPV (G = 1000 W / m^2 T = 298.2 K)

Since we noticed that in Figure 4, for a simulated sunlight of G = 1000 W/m², the current Isc is equal to 4.8A for a value of the open circuit voltage close to 21V.The power is reached to climax (17 V, 75 W). As against the maximum power reached is close to 75 W and voltage 17 V (maximum: Vmp) correspond to the characteristics of the PV array (Table 1). That said, the features that are simulated I (V) and P (V) of GPV are in perfect agreement with the manufacturer data (Table 1). This leads to say that digital model that was the basis for this simulation reflects the physical processes governing the GPV.

Simulation of panel group (GPV)

The GPV of LRAER is performed to obtain a voltage compatible with the load. For more tension, it was assembled Ns modules in series, by cons for the generated current, Np number of parallel modules has been added, serial and parallel protection diodes protect the circuit against the current return.

The characteristics in Figure 5 of the series connection of the panels and has an open circuit voltage equal to the sum of the voltages to the four panels, 84 V and a short-circuit current equal to the sum of short currents - individual circuits of the four panels, that is to say, it is close to 19.2 A. this means that the physical phenomena that were recorded for a panel, have been renewed for the panel group (Figure 5).

Influence of the resistance Rs for GPV, (G = 1000 W/m^2, T=298.2 K)

The series resistance acts on the slope of the

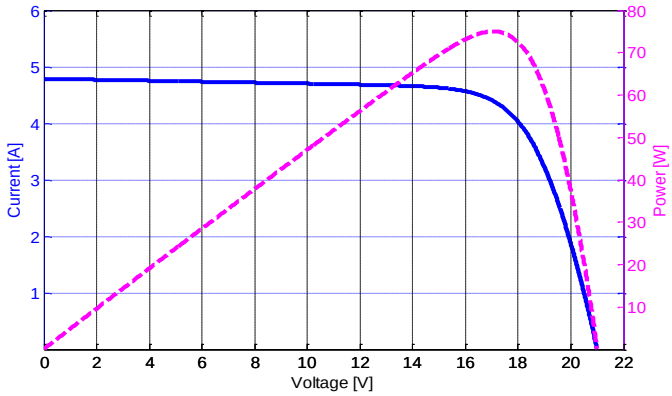

Figure 4. Simulation I (V) and P (V) of the MC model, for one panel (Single diode).

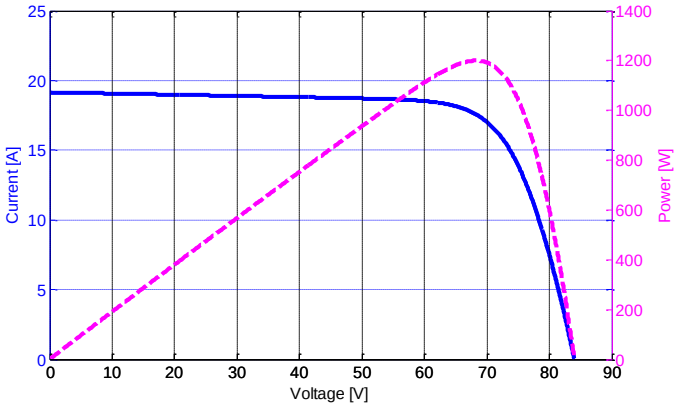

Figure 5. Simulation I (V) and P (V) MC model of panel group (Single diode).

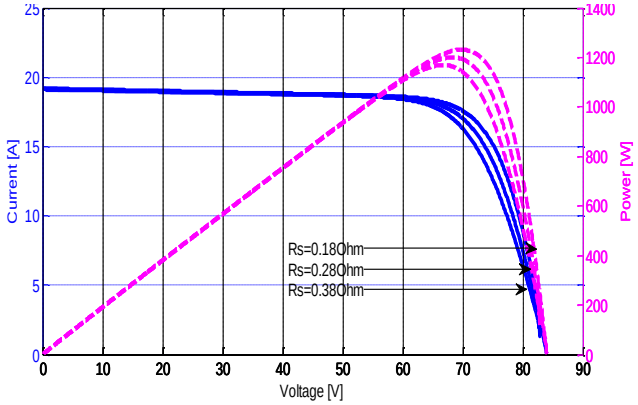

Figure 6. Simulation I (V) and P (V) MC model of panel group for different values of Rs = [0.18, 0.28 and 0.38] Ohm (Single diode).

characteristic, Figure 6, without apparent influence in the area where the panel behaves as a current generator (right near 19 A) against, it acts with an apparent influence on the slope of tension, and when it is high, it

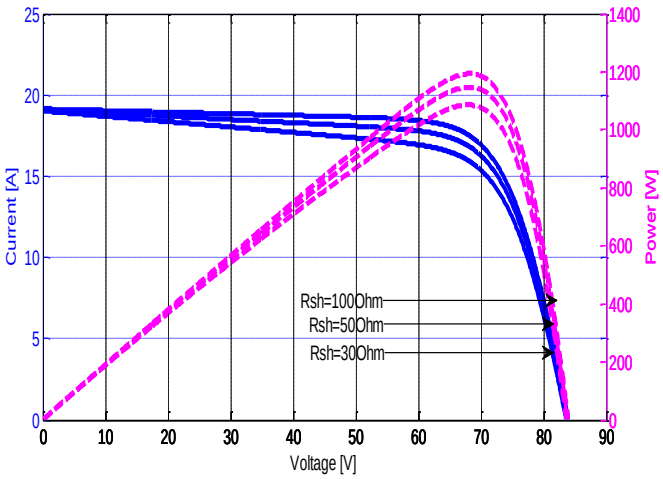

Figure 7. Simulation I(V) and P(V) MC model of panel group for different values of Rsh = [30, 50 and 100] Ohm (Single diode).

decreases the current value of short circuit. Power degrades with increase of the series resistance. A small change in P (V) is noticed to the right of the feature, significantly, the color pink, gives the line. Also note that in general, the performance of a photovoltaic panel is even more degraded than Rs is great.

The simulation is performed and found a very good correlation between simulation results to the manufacturer. They are consistent with the physical phenomena recorded in the literature.

Influence of the resistance Rsh for GPV, (G=1000 W/m^2, T=298.2 K)

The shunt resistance is directly related to the manufacturing process, and its influence is felt as current values that are close to the short-circuit current. The Figure 7 shows that this influence is reflected by an increase in the slope of the curve I (V) GPV in the area corresponding to operation as a current source. This is because it takes subtracting the photocurrent, besides the direct current diode, an additional current varies with the voltage developed. For the curve P (V) changes Rsh is carried out in the same zone as I (V). Thus, it has been noticed that the influence of the shunt resistor which has been translated through the parameters that have been extracted is in agreement with the physical phenomena.

Influence of sunshine on I(V) and P(V)

The simulation results of the characteristics I (V) and P (V) GPV are made to see the influence of the sunshine, this is obtained by fixing the ambient temperature (T = 25°C) and varying sunshine in an appropriate range.

The Figure 8 shows the influence of sunlight on the characteristic I = f (V). If a constant temperature is maintained, we see that the current undergoing a major change, but against the voltage varies slightly.

Because the short circuit current is a linear function of the illumination while the open circuit voltage is a logarithmic function. We varied the level of sunshine G and traced the GPV features.

The Figure 8 illustrates the variation of the power delivered by the generator function of the voltage for different illuminance values which allows us to infer that the physical phenomena recorded in this case it's in perfect agreement with those of the literature and specifications of the manufacturer. There by that the numerical model (MC) and its parameters are extracted correctly reflect the physical phenomena in the case of the influence of illumination on the characteristic I (V) and P (V).

Influence of temperature on I(V) and P(V)

The GPV is constructed so that it is sufficient to obtain a voltage compatible with the load. To illustrate better this, remember, the Boltzmann equation gives: Is = Io exp (eVo / kT).

Experience shows that the open circuit voltage of a solar cell decreases with increasing cell temperature. We present in Figure 9, the characteristic I (V) of GPV for a given level of sunshine G and varying temperatures. The short circuit current, by cons, increases slightly with the temperature on the GPV. Figure 9 further shows the influence of temperature on the characteristic I = f (V). It is essential to understand the changing effect of the

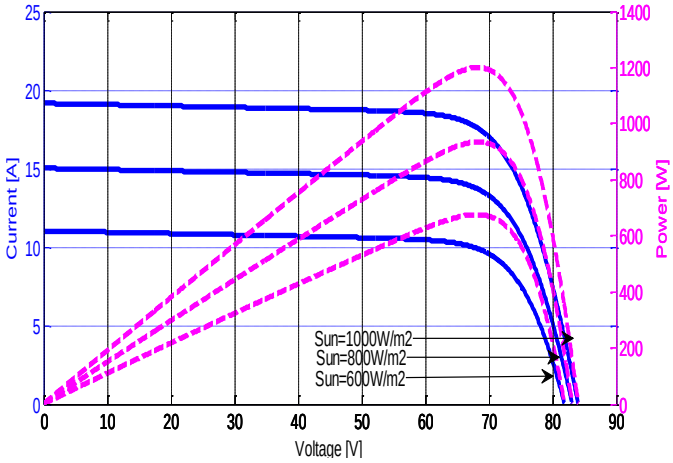

Figure 8. Simulation I (V) and P (V) MC model of panel group for different values of Sun = [600, 800 and 1000] W/m^2 (Single diode).

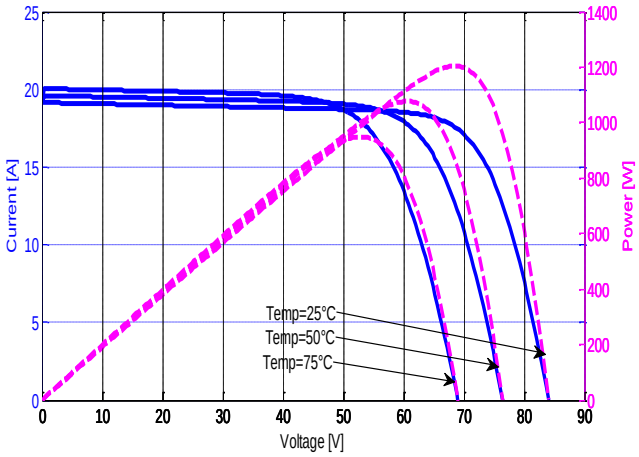

Figure 9. Simulation I(V) and P(V) MC model of panel group for different temperatures Temp = [25, 50 and 75]°C (Single diode).

temperature of a GPV on the characteristic I = f (V).

The current depends on the temperature, since the current increases slightly as the temperature increases, but the temperature negatively affects the open circuit voltage. When the temperature increases the open circuit voltage decreases. Therefore, the maximum power of the generator undergoes a decrease. The power curve P (V) in Figure 9 also illustrates the variation of the power delivered by the generator depending on the voltage for different values of the temperature, which allows us to infer the influence of temperature on the characteristic P (V) and in perfect agreement with the physical phenomena encountered in the literature (Alrashidi et al., 2011; Zadeh and Rezazadeh, 2013; Villalva et al., 2009). This, once again confirms that the digital model and its parameters are extracted illustrate the operation of the GPV.

Validation by comparing the generated and simulated powers

Thus, if in Part Result of Simulation, it was observed that the numerical model reflects the physical phenomena in the form and not to mention the exact meaning which governs the operation of GPV known in the literature. Furthermore, it is important to check their behavior by comparing the experimental and simulated powers during the most remarkable days in order to comment on the accuracy of the numerical model (MC) used in this work.

Table 3. Comparison of absolute errors for the MC model in STC.

Parameter	Manufacture data	MC Model	Relative error
Short circuit current (A)	4.8	4.7885	0.011
Open circuit voltage (V)	21	20.93	0.07
Maximum current (A)	4.4	4.3891	0.011
Maximum voltage (V)	17	17.09	0.09
Maximum power (W)	75	75.09	0.09

Table 4. Comparing errors, the simulated power and real power hang three days.

	Relative errors		
	First day	Second day	Third day
8 :00	0.8092	1.991	1.808
9 :00	2.307	0.6603	0.75
10 :00	0.2778	0.5654	0.4715
11 :00	0.6899	0.6792	0.7606
12 :00	0.6358	0.6467	0.6932
13 :00	0.5862	0.63	0.595
14 :00	0.6785	0.5249	0.6479
15 :00	0.4904	0.47	0.45
16 :00	0.2847	0.1461	1.727
17 :00	0.55	2.481	1.795
18 :00	1.1119	0.8662	0.4458
19 :00	0.1072	0.0378	0.0339
Error average	0.7107	0.8082	0.8481

In addition, the idea sought to consolidate it was given in Table 3 for comparison, the parameters of the manufacturer of the photovoltaic panel and the MC model.

In this part, it was verified if the model (MC) was able to predict the PV system performance in terms of power. And to validate the model, we chose three typical days (Figures 10 and 11): A sunny day (maximum 720 W, a day a little less sunny (maximum 700 W) and a cloudy day with short periods of irradiation high solar (lower to 600 W). Indeed, the GPV of output power for MC (Figure 9) visually shows a negligible difference between the numerical model and the experimental. We note that the two models (numerical and experimental) is follow to deepen these visual examples, we propose the Table 3, for more precision.

Table 3 provides a comparison between the parameters of the manufacturer of the photovoltaic panel and those of the MC model. Regarding the example of the short-circuit current, the relative error between the data of the manufacturer and the model MC, respectively 0.011 for the short-circuit current, and 0.07 for the circuit voltage which shows that our model reflects the actual behavior of the system LRAER.

By cons, in Table 4, we give a comparison, experimentally recorded parameters on LRAER the site for three days per hour and simulated data model MC GPV. With respect, these relative error values, shows the degree of accuracy of the results, through the confrontation of the numerical model and the experimental data. The results are acceptable to prove that the choice of the numerical model (MC) is a conclusive choice.

DISCUSSION

We have in this work, an approach adopted to research the parameters of electrical circuits, considered complex in the literature through the numerical model (MC), which were subsequently validated throughout workflow. The equations that were developed previously for the MC method of the current-voltage characteristic parameter calculations were simulated in the Matlab environment for the test module ATERSA 75 W and the GPV of the LRAER system. It is important to note that not only has been proposed electrical circuit and the corresponding numerical model to a panel of GPV LRAER, but it was

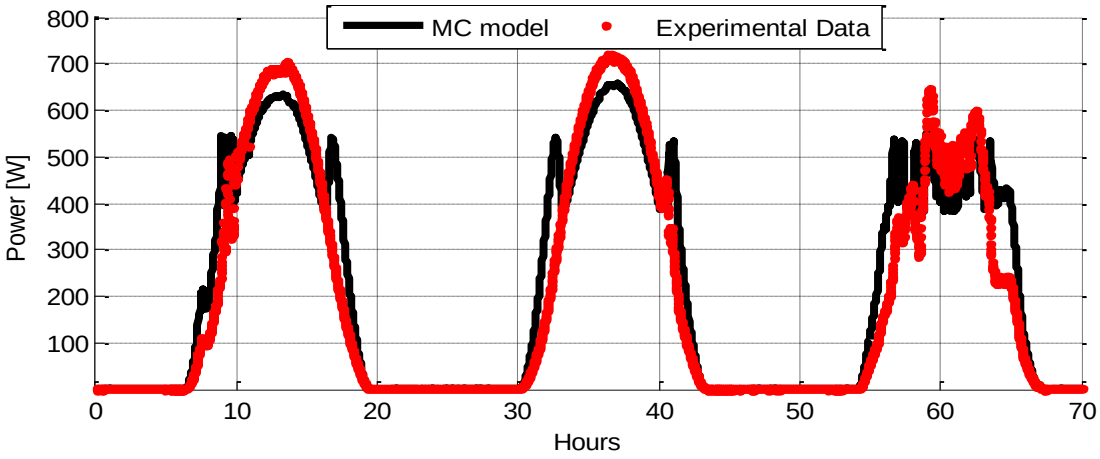

Figure 10. Comparison between the simulated power of the MC model and the experimental power for 3 days.

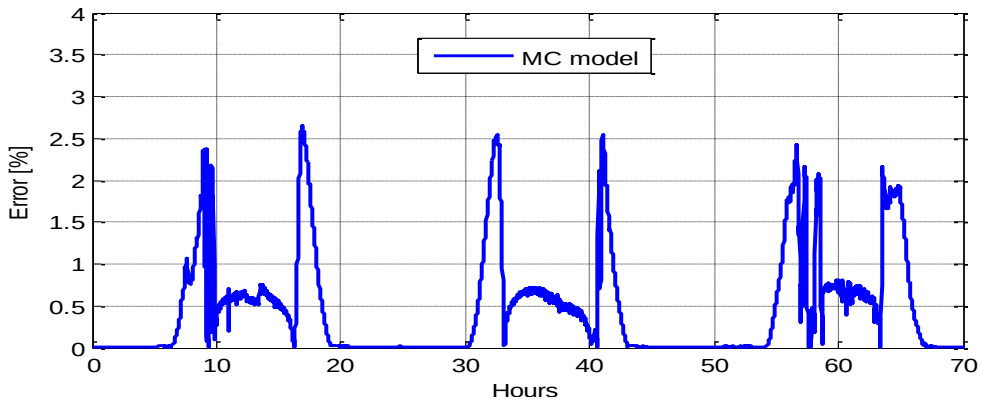

Figure 11. The relative error of the MC model.

extracted parameters, to apply later in a similar way for grouping. Then it was carried out simulations for a panel and the GPV Group of LRAER.

The results were compared with those supplied by the manufacturer. The remarks were reported in the figures that were simulated the characteristics given points for the short-circuit current and open circuit voltage are the same with those given by the manufacturer, without forgetting the details that are registered to the point maximum power.

To strengthen these results, it was conducted comparing the results obtained by simulation (MC) and the experimental results are from the experimental site, it was found that the GPV performance results depend largely on temperature, sunlight of resistance Rsh and Rs and these results are consistent with the physical phenomena already observed in the literature to comfort our approach. Simulation results also comforted the digital model because they have the physical phenomena that are recorded in the literature for this type of installation. In the end, it was made a comparison in terms of errors between the simulation of the power of the numerical model and the results of experimentally recorded parameters on LRAER site. This comparison showed a perfect agreement that strengthens the performance of our model.

Conclusion

This paper presents the modeling of GPV through the model (MC) to describe its behavior in the conditions of use in the Sahel. The MC resolution method was presented in detail. She identified various specific parameters of GPV. The numerical model (MC) that was presented was also used to simulate all the features shown in the various Figures 4 to 11. Each time, a comparison was undertaken with the results of simulations and data from the manufacturer for the test module ATERSA 75 W and those of the GPV of the

LRAER system, to conclude with great accuracy on the compliance of results with those are known in the literature.

The small differences that are sometimes recorded do not create a disagreement with the results that were obtained. The physical phenomena observed in the simulations are in perfect agreement with those noted by the researchers of the discipline.

Conflict of Interests

The authors have not declared any conflict of interests.

Nomenclature: STC, Standard test condition; GPV, Generator Photovoltaic; I, current provided by cell; K, Boltzmann's constant (1.38.10-23 Joules / Kelvin); T, temperature of cell in Kelvin; V, the voltage across the cell; R_S, The series resistance; N_s, Number of cell; I_d, The current of PN junction of the diode; E_s, sunshine in the panels of group (W/m^2); I_{Ph}, Current-photon of the cell; T_j, Junction Temperature cell (°C); I_G, current provided by panels (A); V_G, Tension in the terminal group (V). (V); I_{Sat}, Saturation current; A, Ideality factor; Eg, gaps energy; Eref, Sunshine of reference $1000W/m^2$; Tref, Sunshine of reference at 25°C; q, Elementary charge (1;6.10-19C); P1, P2, P3, P4, P5, are constant parameters.

REFERENCES

Alrashidi MR, Alhajri F, El-naggar KM, Al-othman KA (2011). A new estimation approach for determining the I-V characteristics of solar cells. Sol. Energy 85:1543-1550.

Belhadj R, Benouaz CA, Bekkouche SMA (2010). Estimation de la puissance maximale produite par un générateur photovoltaïque. Rev. Energies Renouvelables 13(N°2):257-264.

Bonkoungou M, Koalaga Z, Njomo D (2013). Modeling and simulation of photovoltaic module considering single-diode equivalent circuit model in Matlab. Int. J. Emerg. Technol. Adv. Eng. 3(3):493-502.

Chenni R, Makhlouf M, Kerbache T, Bouzid A (2007). A Detailed Modelling Method forPhotovoltaic Cells. Energy 32(N°9):1724-1730.

Dumbs C (1999). Développement d'outils pour l'analyse des systèmes hybrides photovoltaïques diesel' : Ecole des Mines de Paris, 1999.

El Ouariachi M, Mrabti T, Tidhaf B, Kassmi K (2009). Regulation of the electric power provided by the panels of the photovoltaic systems. Int. J. Phys. Sci. 4(5):294-309.

Gergaud O, Multon B, Ben Ahmed H (2002). Analysis and Experimental Validation of Various Photovoltaic System Models. Electrimacs Aug 2002, Montreal, Canada. 6 p.

Khazzar R, Zereg M (2010). Comparaison entre les différents modèles électriques et détermination des paramètres de la caractéristique I-V d'un module photovoltaïque. Rev. Energies Renouvelables 13(N°3):379-388.

Villalva MG, Gazoli JR, Filho ER (2009). Comprehensive approach to modeling and simulation of photovoltaic arrays. IEEE Trans. Power Electron. 24(5):1198-1208.

Yahfdhou A, Mahmoud AK, Youm I (2013). Modeling and optimization of photovoltaic generator with Matlab/Simulink. Int. J. I Tech. E Eng. 3(4):108-111.

Yahya M, Kader A, Iyoum A (2011). Behavior and performance of a photovoltaic generator in real time. Int. J. Phys. Sci. 6(18):4361-4367.

Zadeh AA, Rezazadeh A (2013). Artificial bee swarm optimization algorithm for parameters identifications of solar cell modules. Appl. Energy 102:943-949.

Zhou W, Yang H, Fang Z (2007). A novel model for photovoltaic array performance prediction. Appl. Energy 84:1187-1198.

academicJournals

Vol. 11(24), pp. 336-346, 30 December, 2016
DOI: 10.5897/IJPS2016.4541
Article Number: 4E9448962068
ISSN 1992 - 1950

http://www.academicjournals.org/IJPS

International Journal of Physical Sciences

Full Length Research Paper

Sandwich panels from cork and polyester in presence of epoxy resin as interfacial adhesive

C. Belkacemi* and B. Bezzazi

Research Unit Materials, Processes and Environment (URMPE) quoted Frantz Fanon, 35000 Boumerdes, Algeria.

Received 25 July, 2016; Accepted 11 November, 2016

This work presents an experimental study to determine the mechanical properties in bending, tension, compression and shear of a new sandwich material based on natural materials (jute and cork). The sandwich material is made basically of natural materials whose soul is agglomerated cork white (located in Jijel, East of Algeria) and the skins are woven jute with ortho phthalic polyester resin. Agglomerated white cork granules with medium density were used (cork boards with thicknesses of 10, 20 and 30 mm). The bending tests were performed on standard samples that were cut elaborate sandwich plates. The sandwich material prepared was tested for 3 and 4 flex points which indicate the stress, strain, bending stiffness, shear strength and failure mode. It was also found that a core thickness of 10 mm has better results compared to 20 and 30 mm. The results of this study allow us to develop a variety of agglomerated cork white product in for the development of low-density sandwich panels for use in the field of insulation and field of construction.

Key words: Cork, jute, resin, sandwich, mechanical characteristics.

INTRODUCTION

The use of composite materials is increasingly spreading. Their main characteristics include low density, high strength, high stiffness and excellent hardness, which are the requirements in areas such as aerospace, automotive, navigation, construction, etc. Sandwich materials are among the most widely used composite materials. These materials generally consist of: two soles or skins, low thickness with high strength and a much thicker core with low density.

Sandwich structures have increasingly become structural and non-structural components in construction. Sandwich structures are usually based on two thin face sheets with high stiffness and strength, and light-weight core that maintain the distance between the faces and sustains deformation, often with insulation properties. By varying the material and thickness of core and face sheets, it is possible to obtain sandwich structures with different properties and performance (Steeves and Fleck, 2004; Allen, 1969; Zenkert, 1997).

The properties of interest for core materials include, among others, low density and good thermal and acoustic insulation characteristics (Zenkert, 1997; Vinson, 1999). Commonly used core materials are honeycombs, foams and balsa wood, but other alternatives of cellular core structures are being proposed. The cork is a natural cellular material with a set of properties that largely fulfills

*Corresponding author. E-mail: mekki-cherifa@yahoo.fr.

the requirements for sandwich cores. It has an alveolar structure similar to a honeycomb, with closed cells, low density and excellent insulation properties (Pereira, 2007; Pereira et al., 1987; Gibson et al., 1981). It is also a renewable raw material from a sustainable production system, therefore, contributing to the present intent of increasing the ‘‘greenness’’ of construction.

Cork agglomerates are cork-based products that are marketed for several applications, mainly for surfacing, flooring and insulation purposes. The so-called compositions of corks are made with cork granules of variable dimensions that are joined together by using adhesives (e.g. polyurethane, melamine) (Gil, 2009). Although, the composition of cork agglomerates retain most of the properties of the cork material, as summarized in Pereira (2007), the mechanical strength of a specific composite cork product is also related to the properties of the adhesive.

The mechanical behavior of agglomerated cork was characterized for compression (Moreira et al., 2010; Gameiro et al., 2007), tensile (Moreira et al., 2010), shear (Reis and Silva, 2009), three-point bending (Reis and Silva, 2009; Kim and Wallace, 2010; Silva et al., 2010), creep in compression (Mano, 2007), as well as for dynamic compression (Reis and Silva, 2009; Gameiro and Cirne, 2007) and vibrations (Moreira et al., 2010). A few studies already considered cork agglomerates as core materials in sandwich panels. Static bending and shear tests on carbon/epoxy-cork sandwich samples showed that the cork performance depends mainly on density and grain size, with the maximum force, shear strength and modulus increasing with grain size (Reis and Silva, 2009). A comparison between the mechanical behavior during impact of sandwich plates with foam core and cork core showed a larger maximum impact force for the cork core panels with a higher capacity to absorb the impact energy with low depth damage (Castro et al., 2010). Micro-agglomerated cork materials were incorporated as cores in sandwich structures with aluminum alloy face sheets and tested under compression and high pulse wave, which showed that the impulse transmitted to the structure decreased with the core thickness with a threshold core thickness separating sandwich and plate behavior (Sousa-Martins et al., 2013).

This study focuses on the development of sandwich panels with face sheets of laminates with jute fiber and epoxy resin and agglomerated cork as core, including multilayered design. Three types of sandwich panels were produced and tested under compression, tension, bending and shear. The influence of the thickness of the soul of sandwich panels on the mechanical behavior of the sandwich panels was analyzed.

The underlying objective is to use natural local materials to the production of sandwiches with panels of ecological footprint and environmental production of sandwich panels which are light and show good insulation performers, low cost, for partitioning use in construction or interior walls of separation.

In this context, we mechanically characterize a new composite sandwich core of cork and laminate jute/polyester.

This study will focus on the use of a white agglomerated cork medium density with different thicknesses.

EXPERIMENTAL PROCEDURES

The development panel sandwiches were made by the compression method (hydraulic press 28 bar with a temperature of 80°C). The skins are made of jute 3 ply folds and the core sinter base cork in density average thickness of 10, 20, and 30 mm.

The adhesion between the agglomerate cork and polyester resin is low and to improve the adhesion between the skin and the soul epoxy resin film was deposited on the soul before filed jute tablecloths for development sandwich panels.

Several tests on the cork-based sandwich panels obtained as soul and jute/polyester resin as reinforcement are made on a universal machine of the type Zwick 250, piloted by computer with the acquisition testXpert V9.0 software, with a sensor of 250 kN force. The following tests were performed: compression perpendicular, perpendicular traction, pure compression and buckling, three and four points bending and shear test, according to French standards, respectively, NF T54-602 (1983), NF T 54-603 (1983), NF T54-604 (1986), NF T54-606 (1987), and NF T 54-605 (1983). Figure 1 shows the bending tests 3 and 4 points.

Several tests conducted the same type of sandwich to see the influence of thickness. Figures 4, 5 and 6 shows several curves (moving force) sandwiches with different thicknesses of cork (10, 20 and 30 mm). Some sandwiches designated S10, S20 and S30 according to the corresponding thickness will be presented in the next sections.

The normal stress σ3 and σ4 respectively for 3 and 4 bending points are expressed in N/mm². These constraints are also called tensile strength or compression soles according to standard NF T 54-606, they are represented by the following Equations 1 and 2:

$$\sigma 3 = \frac{P1d1}{2es(h+ea)b} \quad (1)$$

$$\sigma 4 = \frac{P2d2}{4es(h+ea)b} \quad (2)$$

where σ: (MPa); P1: maximum effort (N); P2: maximum effort (N); d1: distance between supports (mm); d2: distance between supports (mm); es: thicknesses soles (mm); ea: thickness of the soul (mm); h: height (mm); b: width (mm).

Compression perpendicular test

The test of the compression in the perpendicular direction carried out was with samples of 50 × 50 mm^2 (length × width) (Figure 1) at a constant crosshead speed of 4 mm min^{-1}. The elastic modulus was determined entre 2.5% deformation (ε1) and 7.5% (ε2). The stress at 10% (σ10) was calculated matching ε = 10%. The maximum stress (σmax) achieved during the test was about 1 MPa and the crush value (Delta h max) for this load corresponds to a maximum deformation of about 70% (εmax). After the test, the samples were kept in the laboratory environment for 14 days, after-the thickness of the panel was measured to calculate the relaxation

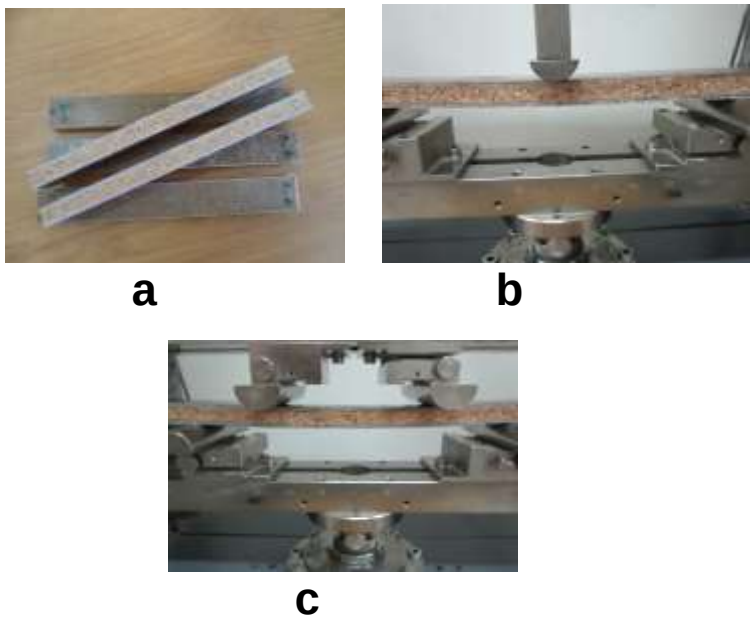

Figure 1. Bending tests: (a) specimens sandwiches; (b) three-point bending; (c) four-point bending.

rate (η). The following mechanical properties were calculated from the stress-strain curves:

$\varepsilon max = \Delta h max h_0 \times 100$ (3)

$Ea = F2 - F1 \Delta h2 - \Delta h1 \times h_0 S_0$ (4)

$\eta = hf2 - hf1 \; hf1 \times 100$ (5)

Perpendicular tensile test

The trial focused on determining the tensile strength perpendicular to a sandwich structure; according to standard NF T 54-603 (November 1983) (Silva et al., 2010). The test consists in subjecting the specimen to a normal tensile strength to the soles of the sandwich, transmitted to the test pieces by means clustering of fastening devices consist of thick fastener sun deformable blocks, glued on with epoxy resin thesis insoles year. Dimensions of tensile specimens 50 × 50 mm^2 (length × width) were manufactured according to the standard. The tests were performed used universal Zwick machines of the type with a traveling speed of the constant load set at 1.2 mm/min according to standard.

The breaking stress in tension perpendicular was calculated using the Following formula:

$$\sigma_P = \frac{F_R}{S_o} \quad (6)$$

where FR is the strength at break (N) of the sandwich structure; FM is the maximum force (N); S_0 is the initial area of the cross section of the specimen (mm^2). The longitudinal compression tests, with or without buckling were carried out to determine the compressive strength for the two boxes-have-been specified in the standard (NF T 54-604, 1986) (Mano, 2007) compression pure, if the sample length is up to twice the total thickness of the sandwich

Figure 2. Specimen sandwich in the compression test.

structure; compression with buckling if the sample length is entre 10 to 12 times the total thickness of the sandwich structure.

Figure 2 shows Specimen sandwich in the compression test structure, compression with buckling if the sample length is entre 10 to 12 times the total thickness of the sandwich structure.

The samples were cut with a width of 50 mm and a length of 70 and 380 mm, respectively for pure compression and compression buckling. Both ends of rectangular samples were carefully machined to be flat, parallel and perpendicular to the load. The tests were performed at a constant crosshead speed of 0.21 and 1.35 mm min^{-1} respectively for pure compression and compression buckling, respectively. The maximum stress in the compression or deformation of the sandwich structure is expressed in MPa such that:

$$\sigma_M = \frac{F_M}{S_o} \quad (7)$$

where F is the maximum force (N), and S0 is the initial section of the test piece (mm^2).

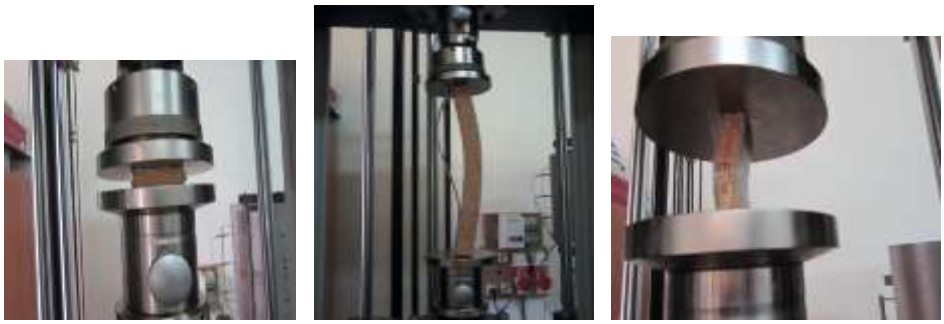

a b c

Figure 3. Test pieces for the tensile test up according to standard (NF T 54-603). Longitudinal compression test with or without buckling.

Module bending stiffness of the sandwich D

NF T 54-606 standard allows, from results of mechanical tests and three four-point bending on sandwiches, defining the flexural rigidity modulus D, the shear modulus N and bending shear modulus Ga soul. Equation 3 gives the value of the modulus of flexural rigidity D (Nmm²).

$$D = \frac{P1\ d1\left[1-\left(\frac{11 d_1^2}{8 d_2^2}\right)\right]}{48 w_1 \left[1-\left(\frac{2 p_1 d_1 w_2}{p_2 d_2 w_1}\right)\right]} \quad (8)$$

Equation 4 defines the shear modulus in bending N expressed in Newtons.

$$N = \frac{P1\ d1\left[\left(\frac{8 d_1^2}{11 d_2^2}\right)-1\right]}{4 w_1 \left[\left(\frac{16 p_1 d_1^3 w_2}{11 p_2 d_2^3 w_1}\right)-1\right]} \quad (9)$$

Equation 5 defines the module of coulomb that the core is related to N by the following equation. It is expressed in Newton's per square millimeter.

$$Ga = N_{4ea/(h+ea)2\ b} \quad (10)$$

Three-point bending

The three-point bending is a mechanical test carried out by placing a beam on two simple supports. According to NF T54-606 Norme (1987), contact between the beam and the support point is considered and located on the ends of the beam. Concentrated in the middle of the beam, the load is applied. The contact between the load and the beam is also considered as a contact point (Tadeu and Santos, 2003).

When the load is gradually increased without exceeding the limit of practical strength; the beam is deformed along a determined arrow, depending on the nature of the constituent components of the beam.

Test device

Bending tests 3 and 4 points are made on a universal machine type Zwick 250 kN. The test was computer-controlled with a 2 mm/min and with a force sensor of 2.5 kN (Figure 3).

Data acquisition is performed with 9.0 V of testXpert software that records the displacement versus force.

Figure 4. Three-point bending tests.

Four-point bending test

This test is performed on the same machine as the three-point bending. According to NF T54-606 Norme (1987), the 4-point bending in particular allows to create a pure bending moment in the central area.

In this case, the same single support is used, but a single two loads concentrated load is applied instead. When the load increases gradually, without exceeding the limit of practical resistance, the beam deforms along and a determined depending on the nature of the constituent components of the beam arrow.

Shear test

The shear tests were performed on a Zwick Universal type machine controlled by a computer 250 kN (testXpert software V 9.0) with a test sample at a speed of 1 mm/min, while equipped with a force sensor of 2.5 kN (Figure 15).

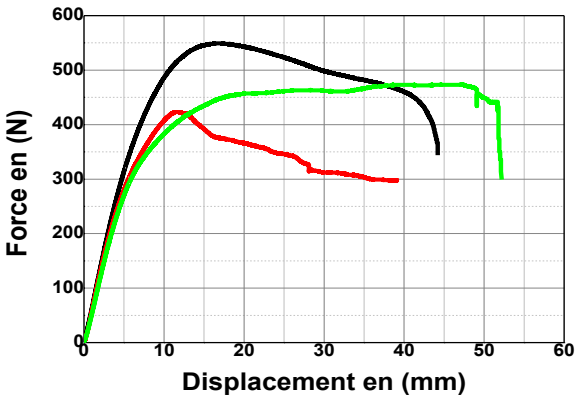

Figure 5. 3 points bending sandwich cork 10 mm.

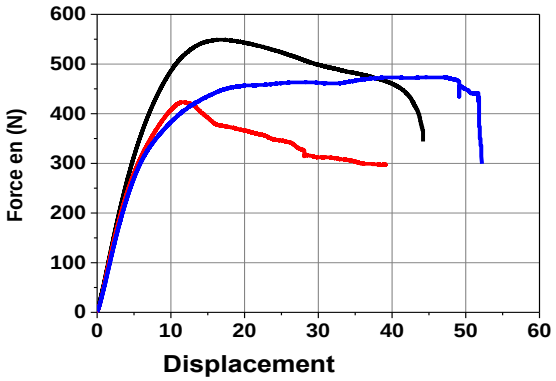

Figure 7. 3 points bending sandwich cork 30 mm.

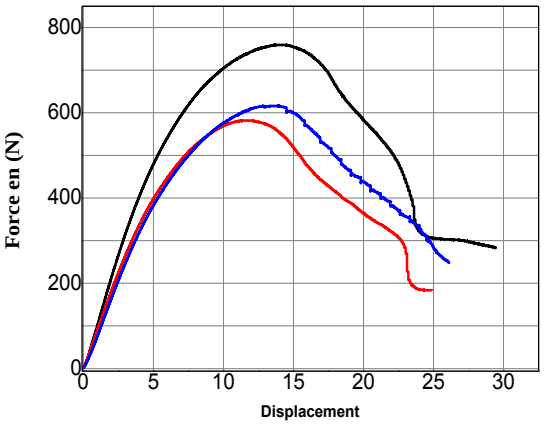

Figure 6. 3 points bending sandwich cork 20 mm.

Figure 8. Bending tests three items, after fracture.

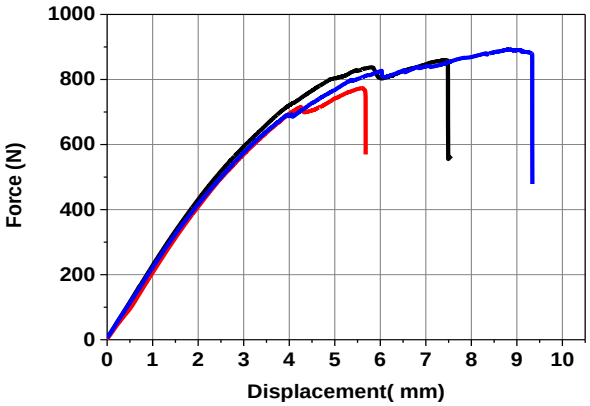

Figure 9. 4-point bending sandwich of 10 mm cork.

Compression with buckling

The three sandwiches have the same behavior towards the longitudinal compression test (with buckling) which is illustrated from the same shape of the curves S10, S20, and S30.

The maximum stress, compression, for each of the variants is: 10.27 MPa for an elongation of 3.42%, for the sandwich S10, 6.47 MPa for an elongation of 3.07% for the sandwich S20, and 4.14 MPa for an elongation of 2.191% for the sandwich S30.

These values show that the increase in thickness of the core causes a reduction of the maximum compressive stress. Therefore, the maximum stress corresponding to S10 is greater than 5% relative to that corresponding to S20 and the latter is greater than 18% relative to that corresponding to S30.

For the sandwich panel skins jute/polyester agglomerated cork and soul, subjected to longitudinal compression test, there is a separation between the skins (laminated jute/polyester) and soul (agglomerated cork) (Figure 7).

Most tests have shown a release of the skins of the core (cork) and producing a separation rupture which finishes with a break skins and a cork buckling subsequently break thereof (Figure 8). This behavior is justified by the poor adhesion of the laminated jute/polyester as sandwich skins and the cork core and the epoxy resin film deposited on the cork did not alter adhering a significantly causing delaminating (Figures 9, 10, 11 and 12).

Pure compression

Compression test

The curves show the first phase, the linear increase of the applied load corresponding to small deformations, followed by a nonlinear.

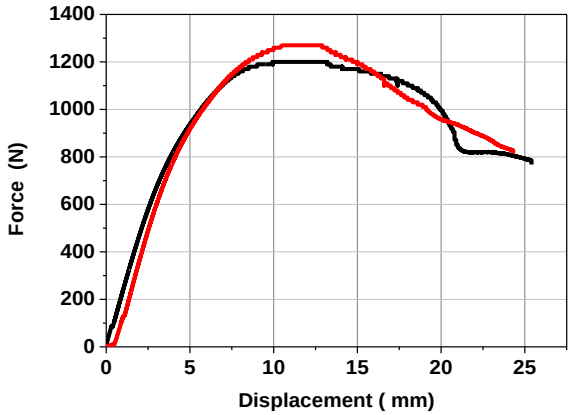

Figure 10. 4-point bending sandwich of 20 mm cork.

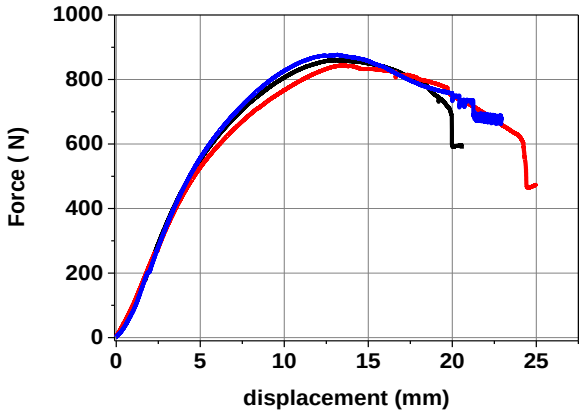

Figure 11. 4-point bending sandwich of 30 mm cork.

Figure 12. Bending tests. Four points: (a) before fracture, (b) after fracture.

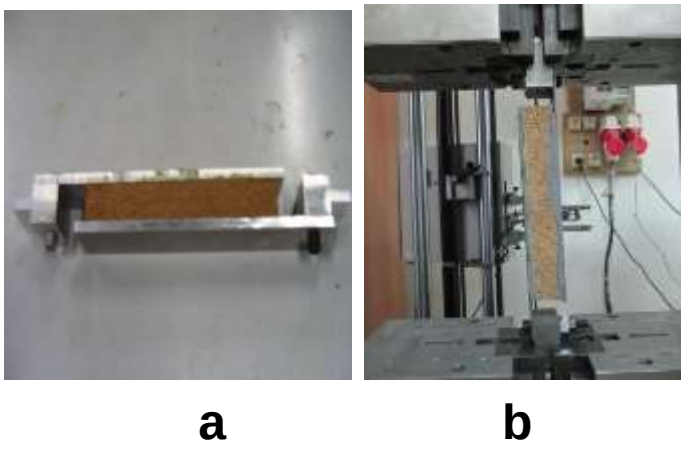

Figure 13. (a) Plate cork attached to two; (b) Test setup for shear traction machine non-deformable metal supports.

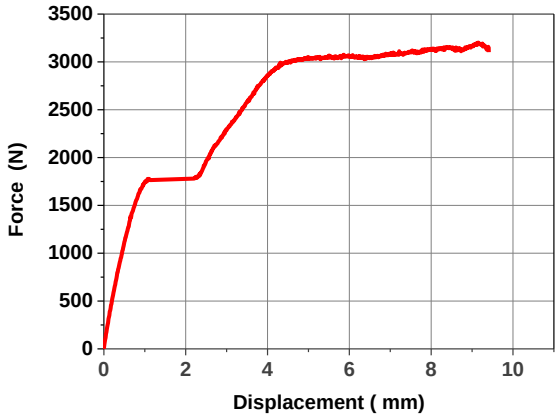

Figure 14. Shear sandwich (10 mm).

Shear test

The shear tests were performed on a Zwick Universal type machine controlled by a computer 250 kN (testXpert software V 9.0) with a test sample at a speed of 1 mm / min while equipped with a force sensor of 2.5 kN (Figure 13). The tested samples were cut with a wire saw according to NF T 54-605 with dimensions: 250 × 50 × 30 mm. The sample is attached to the mechanical jaws of the machine with the two non-deformable metal supports. During loading, the displacement and applied load are recorded.

Several pieces of sandwich materials S10, S20 and S30 are tested. Figures 13, 14, 15 and 16 show the achieved assembly for testing shear.

Perpendicular compression

Table 1 gives the values of the three normal bending stress and four points and σ 4 σ 3 and the flexural rigidity D and the shear stiffness of the modulus N and the core coulomb Ga, for different sandwich structures, with 10, 20 and 30 mm thickness of the core.

Table 2 gives the principal properties of panel sandwiches after the test of compression perpendicular, such as modulus of elasticity (Ea), maximum deformation (εmax [%]), maximum stress (σmax [%]), and relaxation rate η [%].

In all tests, the curves followed the same trend: an elastic deformation zone to values of about 4.73 and 4.91% for S20 and

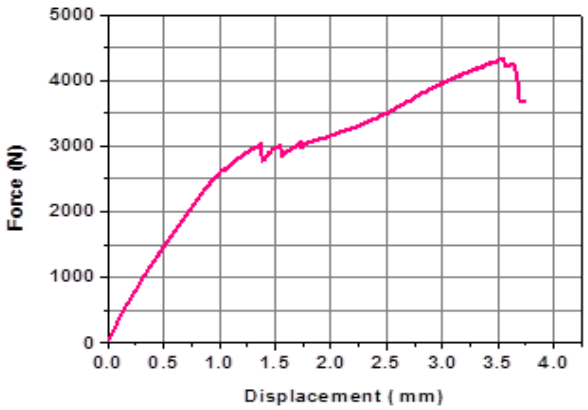

Figure 15. Shear sandwich (20 mm).

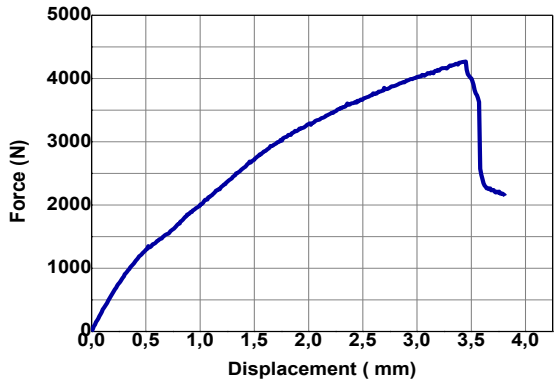

Figure 16. Shear sandwich (30 mm).

S30, respectively, corresponding to 0.896 MPa stress values and 0.915 MPa, respectively, followed by a large platter with a lower slope for deformations of 40 to 50%, with a sharp subsequent rise to higher stresses with deformations for crushing and the cells collapse. The trial was stopped at a stress of 40 and 54 MPa, which corresponds to a deformation of 60 to 64% for S20 and S30, respectively (Figure 17). The effect of the maximum compressive stress in expanded cork agglomerate of the soul of sandwich is as shown in Figure 18.

The compression behavior of two sandwich panels (S20 and S30) showed some differences, but the shape of the stress-strain curve is quite similar, the S10 sandwich panels have shown a module larger than the sandwich panels S20 and S30 (2.3 and 2.4 MPa). Relaxation rate after 14 days was lower for SN20 panels S30 and S10 relative to the panels (80 and 70%, respectively).

Compression with buckling

The three sandwiches have the same behavior towards the longitudinal compression test (with buckling) which is illustrated from the same shape of the curves S10, S20, and S30 (Figure 19).

The maximum stress, compression, for each of the variants is: 10.27 MPa for an elongation of 3.42%, for the sandwich S10, 6.47 MPa for an elongation of 3.07% for the sandwich S20, and 4.14 MPa for an elongation of 2.191% for the sandwich S30.

These values show that the increase in thickness of the core causes a reduction of the maximum compressive stress. Therefore, the maximum stress corresponding to S10 is greater than 5% relative to that corresponding to S20 and the latter is greater than 18% relative to that corresponding to S30.

For the sandwich panel skins jute/polyester agglomerated cork and soul, subjected to longitudinal compression test, there is a separation between the skins (laminated jute/polyester) and soul (agglomerated cork) (Figure 20). Figure 21 shows the stress strain curve of sandwich panels in pure compression longitudinal. The testing of shear at early separation and total detachment of the skin of the sandwich is illustrates in Figure 22.

Most tests have shown a release of the skins of the core (cork) and producing a separation rupture which finishes with a break skins and a cork buckling subsequently break thereof (Figure 20). This behavior is justified by the poor adhesion of the laminated jute/polyester as sandwich skins and the cork core and the epoxy resin film deposited on the cork did not alter adhering a significantly causing delaminating.

Pure compression

The curves show the first phase, the linear increase of the applied load corresponding to small deformations, followed by a nonlinear phase short until the maximum load is reached; then a decrease of the load applied to the separation of the skins of the core is observed.

The maximum longitudinal compression stress (pure) for three variants is: 29.46 MPa for an elongation of 1.5 mm, for the sandwich S10; 9.31 MPa for an elongation of 1.2 mm for the sandwich S20; 6.18 MPa for an elongation of 1 mm, for the sandwich S30.

These values show that the increase in thickness of the core causes a reduction of the maximum compressive stress. Therefore, the maximum stress corresponding to S10 is greater than 68.4% relative to that corresponding to S20 and it is greater than 33.6% relative to that corresponding to S30.

RESULTS AND DISCUSSION

Influence of the thickness of the sandwich on the breaking strength

The curves (force-displacement) sandwiches are similar but with different thicknesses (10, 20 and 30 mm) show linear behavior for the S20, then the nonlinear phase to failure to 1200 N for a displacement of 14 mm. The S30 has a linear behavior, then the rupture is 810 N for a displacement of 15 mm. For S10 breaking is 850 N for movement 9 mm.

Analysis of the mode of failure in bending three and four points

Breaking recorded four-point bending on sandwiches is noticed on the web (transverse fracture) (Figure 12). By looking more closely at this cross, as the force is exerted on the sample, there is a crack, which appears above the lower flange, which propagates along the thickness of the sandwich (Figure 12). This failure mode is completely

Table 1. Values obtained by calculation according to the equations given by the standard NF T 54-60.

Sandwich	τ(Mpa)3ts	τ(Mpa)4ts	σ(Mpa)3pts	σ(Mpa)4pts	D (Nmm²)	N(N)	G_a(N/mm²)
S10	0.4016425	0.72697282	12.6642099	11.5027344	661461383.5	11223.3571	13.86419354
S20	0.29515557	0.45242001	11.1505835	8.51694301	41876059.79	651435.072	581.8117141
S30	0.18170106	0.32158918	9.72400223	8.66350172	3851960310	5383.85467	3.717517577

Table 2. Main properties of sandwich panels.

Panneaux sandwiches	Ea [MPa]	σ10 [MPa]	σmax%	εmax [%]	η [%]
S10	6.8	1.94	37.90	23.27	68.54
S20	2.4	1.46	41.50	62.61	89.35
S30	2.2	1.38	54.10	58.22	93.82

SN20 and SN40 in compression perpendicular: Module apparent elasticity (Ea), deformation ε = 10% (σ10) maximum deformation (εmax) and the relaxation rate η [%] (Sousa-Martins et al., 2013).

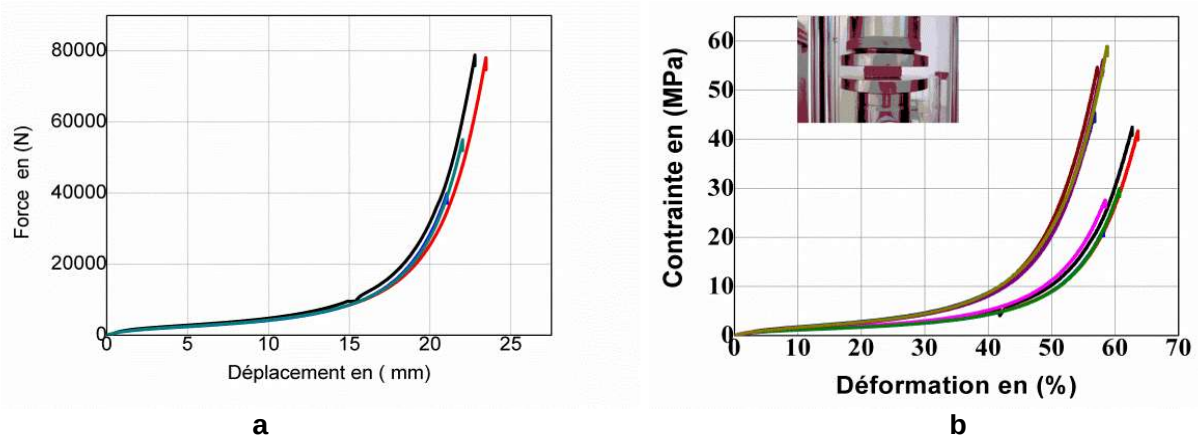

Figure 17. Stress-strain curve of the sandwich panels (S10, S20 and S30) during compression in the perpendicular direction.

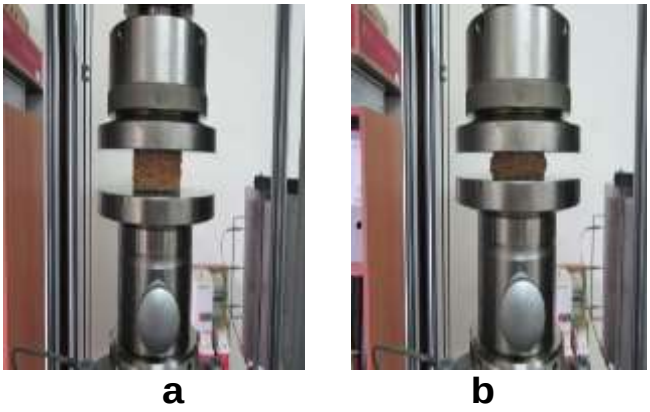

Figure 18. Image of a specimen of S30 sandwich panel before (a) and after (b) compression in the perpendicular direction.

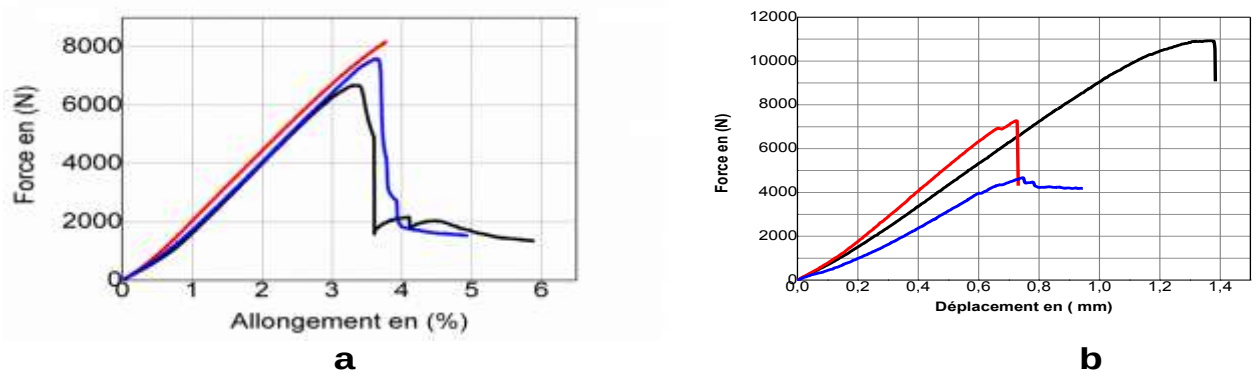

Figure 19. Stress-strain curve of sandwich panels (a): S10 and (b): S20 and S30 during the compression in the longitudinal direction with buckling.

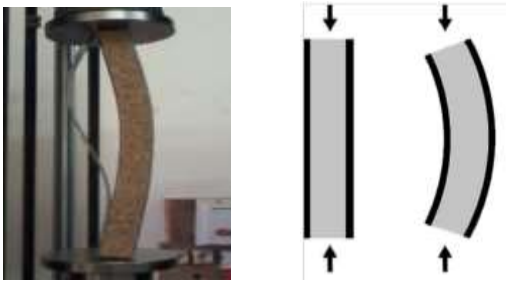

Figure 20. Image diagram of a sandwich test (S30) during the longitudinal compression test with buckling.

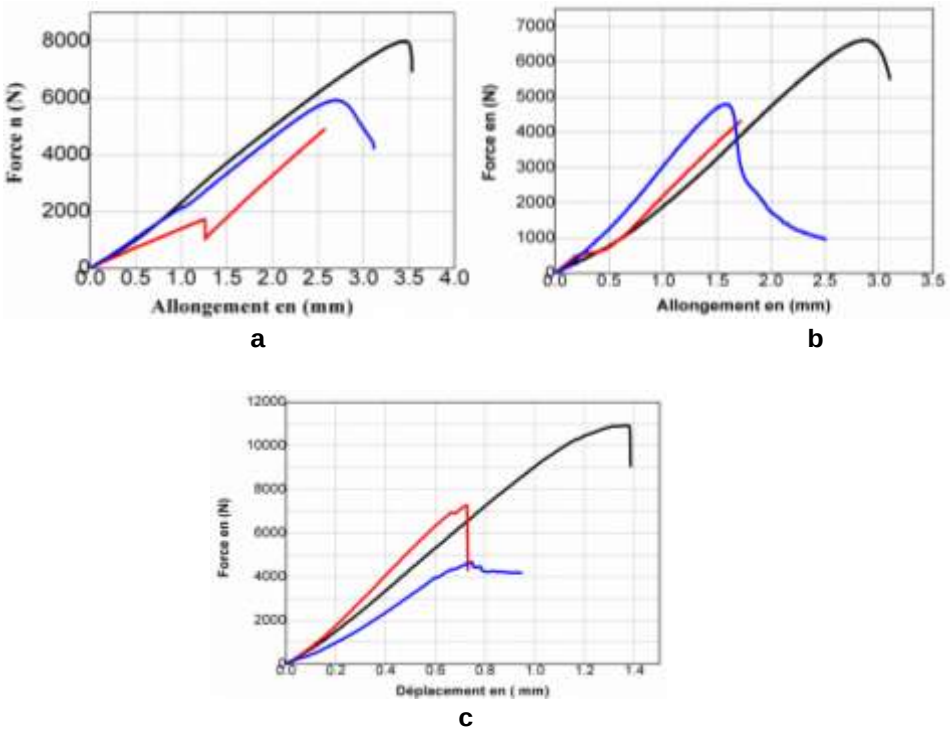

Figure 21. Stress-strain curve of sandwich panels S10, S20 and S30 in the pure longitudinal.

a b

Figure 22. Testing of shear (a) early separation of the skins of the sandwich, (b) the end of testing with total detachment of the skin.

different from that obtained by three-point bending where the web fracture can be observed (Figure 7).

The results from three bending tests and four points, sandwiches on S10, S20 and S30, show that: the normal stress σ bending three points is higher for S10 by almost 12% and S20 by 23.22% compared to S30; the normal stress σ of four-point bending is higher for S10 with 26.18% and for S20 with 24.69% with respect to S30. Another thing was noted for the flexural rigidity (D) and the shear rigidity (N) where it was observed was the highest value given by the variants S30 and S20.

The results of the stress and the maximum shear modulus of sandwiches S10, S20 and S30 from the shear tests according to the NF T 54-606 are not significant as they were observed during the test and after some filling 250 [kgf], peeling skin (Figure 18b) of the soul that is due to poor adhesion between the cap and the polyester resin film and epoxy resin used between the laminates and sandwich core has resist this charge and it has not suffered the shear.

Conclusion

Sandwich structures are designed to be subjected to bending efforts and applied in thermal insulation.

The use of natural fiber such as jute will certainly impact on the environment and adds value to the jute fibers (natural fiber) through a rational and effective implementation in the vast field of composite structures.

The 3 and 4-point mechanical bending tests as well as shear, on sandwiches made of cork with different core thicknesses exhibit good results and shows that the stress, strain, bending stiffness and shear strength of the failure mode are a function of the thickness of the core and the resin depend is likely used to avoid the polyester resin separation from the skins of the soul which was not observed in the case of sandwich-based epoxy resin. No delaminating was observed at the skins, while delaminating between the core and the skins was noticed. To address the problem of low adhesion between the polyester resin and cork epoxy resin film was added on the cork before developing sandwiches which give good results, especially in three and four points bending and even a treatment study on the polyester resin.

Analysis of the fractured surfaces of different sandwiches identified the influence of the thickness of the core. Based on the results found sandwiches with 10 mm thick soul shows the best features compared to those of 20 and 30 mm. Mechanical characteristics and the low mass density of these structures have their own sandwiches advantage suggesting applications particularly in the field of insulation (construction area).

The results of this study allow us to develop a variety of white agglomerated cork produced from jute, in the development of low mass density panels sandwiches in order to use it in the field of insulation (field of construction).

Finally, we believe that this preliminary study should be complemented by a study on the improvement of adhesion between the polyester resin and the surface of the cork using a natural resin to benefit ecological character which can bring significant mechanical improvements in the mechanical and environmental performance of such structures, to replace industrial resins. The use of natural materials available in Algeria such as jute and cork for the development of the composites industry is a key to meet the needs of the habitat. Our study concerns the use of a natural fiber (jute) as well as white agglomerated cork, which has good thermal and sound insulation properties.

Making a panel sandwich among all the natural fibers, jute has interesting mechanical properties in terms of tensile strength, with interesting properties in flexion (Belkacemi and Bezzazi, 2014; Mir and Bezzazi, 2011). In addition, imported raw jute is processed, spun and woven in Algeria, it is available and at low cost.

Conflict of Interests

The authors have not declared any conflict of interests.

REFERENCES

Allen HG (1969). Analysis and design of structural sandwich panels. Oxford: Pergamon Press 1969.

Belkacemi C, Bezzazi B (2014). Quasi-static mechanical characterization and fatigue of a composite laminates. Adv. Appl. Sci. Res. 5(3):328-335.

Castro O, Silva JM, Devezas T, Silva A, Gil L (2010). Cork agglomerates as an ideal core material in lightweight structures. Mater. Des. 31:425-432.

Gameiro CP, Cirne J (2007). Dynamic axial crushing of short to long circular aluminium tubes with agglomerate cork filler. Int. J. Mech. Sci. 49(9):1029-1037.

Gameiro CP, Cirne J, Gary G (2007). Experimental study of the quasi-static and dynamic behaviour of cork under compressive loading. J. Mater. Sci. 42:4316-4324.

Gibson LJ, Easterling KE, Ashby MF (1981). The structure and mechanics of cork. Proc. R. Soc. London A 377:99-117.
Gil L (2009) Cork composites: a review. Materials 2:776-789.
Kim S, Wallace D (2010). Designing and testing of cork composite core material. In: Ravichandran G, editor. 9th International conference on Sandwich Structures 2010.
Mano JF (2007). Creep-recovery behaviour of cork. Mater. Lett. 61:2473-2477.
Mir A, Bezzazi B (2011). Caractérisation mécanique d'un panneau sandwich à âme en liège et peaux jute/époxy. Comptes Rendus des JNC 17 - Poitiers 2011.
Moreira RAS, de Melo FJQ, Rodrigues JFD (2010). Static and dynamic characterization of composition cork for sandwich beam cores. J. Mater. Sci. 45:3350-3366.
NF T54-606 Norme (1987). structures sandwiches à base de plastiques. Essai de flexion.http://www.lavoisier.fr/livre/autre/norme-nf-t-54-606-structures-sandwiches-a-base-de-plastiques-essai-de-flexion/descriptif_1967952
Pereira H (2007). Cork: biology, production and uses. Amsterdam: Elsevier; 2007.
Pereira H, Rosa ME, Fortes MA (1987). The cellular structure of cork from Quercus suber L. Iawa Bull. 8(3):213-218.
Reis L, Silva A (2009). Mechanical behavior of sandwich structures using natural cork agglomerates as core materials. J. Sandwich Struct. Mater. 11(6):487-500.
Silva JM, Devezas T, Silva A, Gil L, Nunes C, Franco N (2010). Exploring the use of cork based composites for aerospace applications. Mater. Sci. Forum 636-637:260-265.
Sousa-Martins J, Kakogiannis D, Coghe F, Reymen B, Teixeira-Dias F (2013). Behaviour of sandwich structures with cork compound cores subjected to blast waves. Eng. Struct. 46:140-146.
Steeves CA, Fleck NA (2004). Material selection in sandwich beam construction. Scr. Mater. 50:1335-1339.
Tadeu A, Santos P (2003). Assessing the effect of a barrier between two rooms subjected to low frequency sound using the boundary element method. Appl. Acoustics 64(3):287-310.
Vinson JR (1999). The behaviour of sandwich structures of isotropic and composite materials. Lancaster: Technomic Publishing Co. Inc. 1999.
Zenkert D (1997). The handbook of sandwich construction. North European engineering and science conference series. Cradley Heath: EMAS Publishing P 442.

International Journal of Physical Sciences

academicJournals